ORIGINAL ARTICLE

# Metal dyshomeostasis in the substantia nigra of patients with Parkinson's disease or multiple sclerosis

Asuncion Carmona[1] | Eleonora Carboni[2] | Lucas Caldi Gomes[3] | Stéphane Roudeau[1] | Fabian Maass[2] | Christof Lenz[4,5] | Richard Ortega[1] | Paul Lingor[3,6,7]

[1]University Bordeaux, CNRS, Gradignan, France

[2]Department of Neurology, University Medical Center Göttingen, Göttingen, Lower-Saxony, Germany

[3]School of Medicine, Klinikum rechts der Isar, Department of Neurology, Technical University of Munich, München, Bavaria, Germany

[4]Bioanalytical Mass Spectrometry, Max Planck Institute for Multidisciplinary Sciences, Göttingen, Germany

[5]Department of Clinical Chemistry, University Medical Center Göttingen, Göttingen, Germany

[6]DZNE, German Center for Neurodegenerative Diseases, Research Site Munich, Munich, Germany

[7]Munich Cluster for Systems Neurology (SyNergy), Munich, Germany

**Correspondence**

Asuncion Carmona, University Bordeaux, CNRS, LP2i Bordeaux, UMR 5797, F-33170, Gradignan, France.
Email: asuncion.carmona@u-bordeaux.fr

## Abstract

Abnormal metal distribution in vulnerable brain regions is involved in the pathogenesis of most neurodegenerative diseases, suggesting common molecular mechanisms of metal dyshomeostasis. This study aimed to compare the intra- and extra-neuronal metal content and the expression of proteins related to metal homeostasis in the substantia nigra (SN) from patients with Parkinson's disease (PD), multiple sclerosis (MS), and control subjects. Metal quantification was performed via ion-beam micro-analysis in neuromelanin-positive neurons and the surrounding tissue. For proteomic analysis, SN tissue lysates were analyzed on a nanoflow chromatography system hyphenated to a hybrid triple-quadrupole time-of-flight mass spectrometer. We found increased amounts of iron in neuromelanin-positive neurons and surrounding tissue in patients with PD and MS compared to controls (4- to 5-fold higher) that, however, also showed large inter-individual variations. Copper content was systematically lower (−2.4-fold) in neuromelanin-positive neurons of PD patients compared with controls, whereas it remained unchanged in MS. Protein–protein interaction (PPI) network analyses revealed clusters related to Fe and Cu homeostasis among PD-deregulated proteins. An enrichment for the term *"metal homeostasis"* was observed for MS-deregulated proteins. Important deregulated hub proteins included hemopexin and transferrin in PD, and calreticulin and ferredoxin reductase in MS. Our findings show that PD and MS share commonalities in terms of iron accumulation in the SN. Concomitant proteomics experiments revealed PPI networks related to metal homeostasis, substantiating the results of metal quantification.

**KEYWORDS**
metals, multiple sclerosis, neuromelanin neuron, Parkinson's disease, proteomics, substantia nigra

---

----------------------------------

## 1 | INTRODUCTION

Iron (Fe), copper (Cu), and zinc (Zn) are essential metals for normal brain function. Their dyshomeostasis, that is, changes in their concentration or local distribution, is observed in many neurodegenerative diseases (Barnham & Bush, 2014; Dales & Desplat-Jégo, 2020; Jellinger, 2013; Mezzaroba et al., 2019). For example, Fe overload is observed in Parkinson's disease (PD), Alzheimer's disease (AD), Lewy body dementia, multi-system atrophy (MSA), progressive supranuclear palsy, Creutzfeldt–Jakob disease (CJD), Friedreich ataxia, Huntington's disease, amyotrophic lateral sclerosis (ALS), and also multiple sclerosis (MS) (Jellinger, 2013; Ward et al., 2014). In PD-affected brains, there is a specific increase in Fe in the substantia nigra (SN), the brain region affected by the neurodegeneration of dopaminergic neurons (Dexter et al., 1989; Hirsch et al., 1991; Jellinger, 2013; Li et al., 2022; Ward et al., 2014). In MS, Fe accumulates in the gray matter, Fe depletion is seen in the normal-appearing white matter, and some studies showed deposition of Fe around the MS lesion plaques (reviewed in Stephenson et al., 2014; Dales & Desplat-Jégo, 2020). The role of Fe overload as a cause or a consequence of neurodegenerative diseases is still debated (Dales & Desplat-Jégo, 2020; Khalil et al., 2011; Ndayisaba et al., 2019; Stankiewicz et al., 2014). Cu is another element with an altered distribution in many neurodegenerative diseases. Cu deficit has been reported in PD and AD brains (Davies et al., 2014; Greenough et al., 2016; Scholefield et al., 2021), while excess Cu is observed in MS, MSA, ALS, and CJD (Dales & Desplat-Jégo, 2020; Jellinger, 2013), and most importantly, in Wilson's disease, where Cu accumulation occurs as a result of mutations in the *ATP7B* gene (Roberts & Schilsky, 2008). Recent research has focused on identifying common molecular mechanisms of metal dyshomeostasis in neurodegenerative diseases, such as newly identified cell death pathways, ferroptosis and cuproptosis (Acevedo et al., 2019; Scholefield et al., 2020).

The metal composition of neuromelanin (NM)-positive neurons is of particular interest for understanding neurodegeneration in PD (Biesemeier et al., 2016; Zucca et al., 2023). NM is a dark pigment that is mostly present in catecholaminergic neurons situated in the SN and the locus coeruleus. In the SN, dopaminergic neurons are NM positive and comprise a neuronal population of particular vulnerability in PD. Chemically, NM is a byproduct of dopamine metabolism that naturally accumulates with age and represents a complex aggregate with the ability to bind Fe and Cu, thus reducing the levels of oxidative stress in neurons (Biesemeier et al., 2016; Zucca et al., 2023). The metal-buffering capacity of NM in the SN might be altered with age (Zecca, Stroppolo, et al., 2004). Our study aimed to compare the multi-elemental composition in NM neurons and surrounding tissue, as well as the expression of proteins involved in metal homeostasis in post-mortem human brains from patients with PD and MS. We performed a combination of ion-beam analytical techniques micro-PIXE/RBS (particle-induced X-ray emission and Rutherford backscattering spectrometry) that offers a high detection sensitivity and accurate quantification of trace elements in biological samples

(Menezes Lyra da Cunha et al., 2016). Particular attention was paid to applying a non-denaturing sample preparation protocol, based on cryogenic methods, to avoid any metal loss or metal contamination (Carmona et al., 2019). In parallel, a proteomic analysis was performed by mass spectrometry to quantify brain tissue proteins in the same patients. This multi-modal approach allowed the identification of not only different but also common molecular mechanisms of metal dyshomeostasis in PD and MS.

## 2 | MATERIALS AND METHODS

### 2.1 | Human brain tissue, ethical approval, and sample selection

Human brain tissue samples and related clinical and neuropathological data were supplied by the Parkinson's UK Brain Bank (RRID:SCR_007030), funded by Parkinson's UK, a charity registered in England and Wales (258197) and in Scotland (SC037554). Informed consent of donors was incurred by the brain bank sample provision. All analyzed samples were sections of snap-frozen tissue blocks from the midbrain region. Ethical approval was given by the Multicenter Research Ethics Committee (07/MRE09/72). The study involves seven control individuals, eight MS patients, and eight PD patients. Further details on the samples used in this study are provided in Supplementary S1. The study was not pre-registered.

### 2.2 | Preparation of human brain tissue samples

Adjacent facing midbrain sections were prepared with a thickness of $30\,\mu m$ in a cryostat at $-17°C$ with a sample holder at $-15°C$ using special Teflon-coated blades (LEICA DB80 LX, cat. no. 14035843497) to avoid contamination by metal particles as a result of friction as adapted from previously published methods (Carmona et al., 2019). For each cryo-section pair, the first was placed onto a microscope slide for histological staining. This tissue cryo-section was then fixed in methanol (Sigma-Aldrich, cat. no. 179337) for 10 minutes at $-20°C$, washed three times in phosphate-buffered saline (PBS, Sigma-Aldrich, cat. no. P5368), and stained with hematoxylin–eosin (H&E, Sigma-Aldrich, cat. no. HT110132). The second cryo-section was left unstained to preserve the native elemental distribution and to avoid metallic contaminations, and deposited onto a special sample holder for micro-PIXE/RBS analyses (Carmona et al., 2019). This sample holder is composed of a polyether ether ketone (PEEK) rigid frame, covered with a transparent ultra-pure polycarbonate film of $2\,\mu m$ thickness. Each tissue section was sheltered with another sample holder to prevent tissue deformation or movement during transfer and analyses. The unstained cryo-sections, maintained between two sample holders, were freeze-dried with a Christ alpha 2–4 LD plus at $-85°C$ under vacuum ($2.5 \times 10^{-3}$ mbar) for 24 h to preserve the structural integrity of the tissues and remove water from samples to allow PIXE/RBS analyses performed under vacuum.

The H&E-stained sections were imaged at the bright-field microscope to identify NM-positive neurons. To precisely locate NM neurons on the adjacent unstained cryo-sections prepared for micro-PIXE/RBS analysis, we used internal markers consisting of orientation marks (pinholes) made with a needle in the tissue, around the regions of interest, before sectioning. Thanks to the position of these markers, we could superpose the images of the two consecutive adjacent facing cryo-sections and unambiguously identify NM neurons on the unstained sections for further micro-PIXE/RBS analysis (Figure 1a).

## 2.3 | Micro-PIXE/RBS analysis

Micro-PIXE and RBS analyses were performed in areas larger than the NM neurons, to determine the element content in the single NM neurons and the area surrounding the NM neurons, referred to as surrounding tissue (Figure 1c,d). This surrounding tissue may contain brain extracellular matrix, neuropil, non-NM-neurons, astrocytes, and glial cells. The elemental content was determined for P, S, Cl, K, Ca, Fe, Cu, and Zn and expressed in $\mu g \cdot g^{-1}$ of dry mass by combining PIXE and RBS analyses as explained hereafter. P, S, Cl, K, Ca, Fe, Cu, and Zn elemental content values for each of the 326 analyses performed are presented in Supplementary S2.

Micro-PIXE and micro-RBS analyses were performed simultaneously using the AIFIRA (*Applications Interdisciplinaires des Faisceaux d'Ions en Région Aquitaine*) particle accelerator facility (Figure 1b) following published protocols (Carmona et al., 2008; Perrin et al., 2015). In brief, the energy of the incident proton beam produced by the Cockcroft–Walton accelerator was set to 3.0 MeV. The beam was focused onto the sample surface to a spot of 2 μm in diameter, resulting in a proton beam current of 0.3 nA as measured with a Faraday cup below the sample. The sample was placed in front of the proton beam at 90°, respectively, to the beam direction. X-ray emission measurements for PIXE analysis were obtained with two identical silicon–lithium Si(Li) energy-dispersive detectors placed in front of the sample on both sides at an angle of +45°. The RBS measurements were performed using a passivated implanted planar silicon (PIPS) detector placed at 135°, respectively, to the proton beam direction. For quantitative analysis, PIXE spectra were treated with
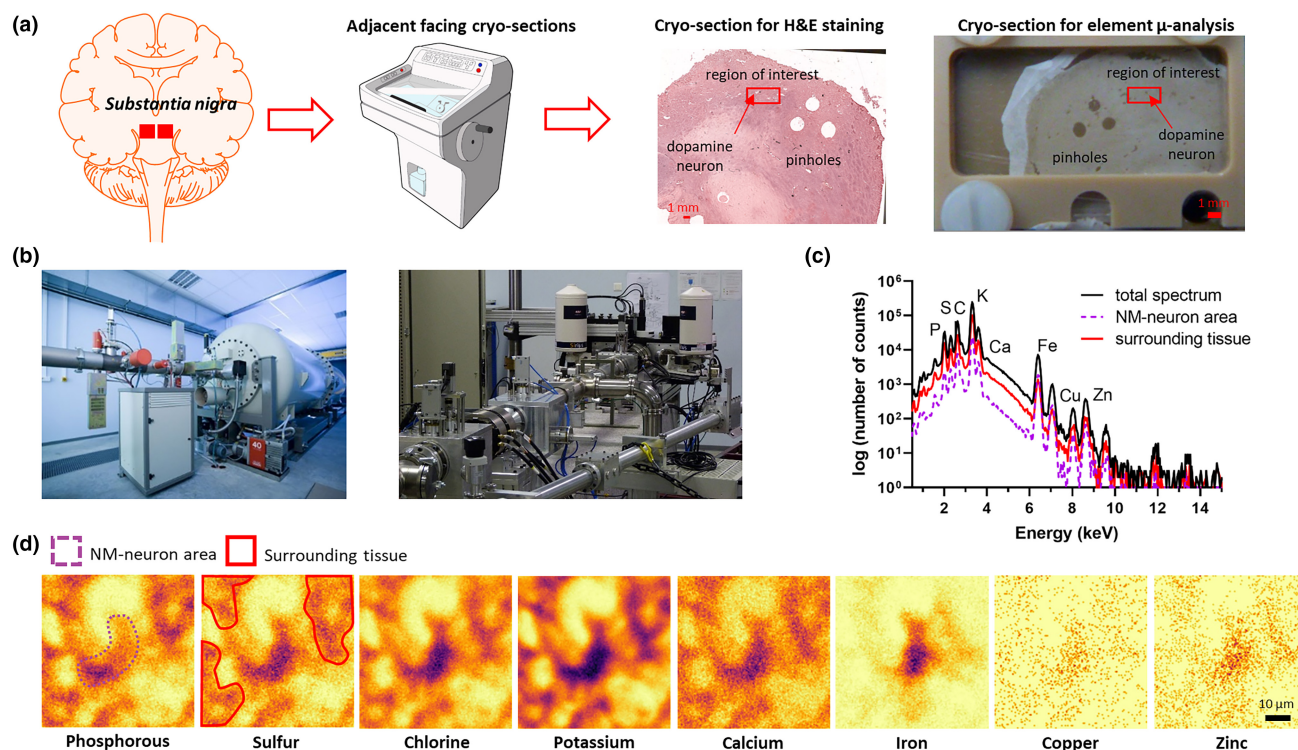


**FIGURE 1** Procedure for brain tissue preparation and micro-analysis. (a) Two adjacent cryo-sections facing each other, one for hematoxylin–eosin (H&E) staining and the other unstained for element micro-analysis, are prepared from frozen SN tissues. Regions of interest containing dopamine neurons are selected from H&E-stained images. Pinholes performed on the tissue before cryo-sectioning are used as internal positioning markers to identify the regions of interest on the unstained section for micro-PIXE/RBS (particle-induced X-ray emission/RBS, Rutherford backscattering spectrometry). (b) Views of the Cockcroft–Walton accelerator at AIFIRA facility and the micro-PIXE/RBS beamline showing the focusing optics at the forefront and the two silicon–lithium Si(Li) energy-dispersive X-ray detectors in the background. (c) Example of PIXE spectra used for element quantification from a region of interest: total spectrum of the analyzed area (in black), spectrum extracted from the NM neuron area (in magenta, dotted line), and spectrum extracted from the surrounding tissue (in red). (d) PIXE elemental distributions from a region of interest with an NM neuron in the center. The selected areas for quantification of the elements in the NM neuron and surrounding tissue are shown in magenta dotted line and red, respectively (see corresponding spectra in (c)).

GUPIXWIN software (Campbell et al., 2010), and the elemental content was calculated as µg of element per cm$^2$ (µg cm$^{-2}$). The corresponding RBS spectra obtained simultaneously were simulated with the SIMNRA program (Mayer, 1997) and the mass of the analyzed areas was calculated and expressed as g of sample per cm$^2$ (g cm$^{-2}$). By applying both techniques simultaneously, the local elemental content expressed as µg of element per g of sample (µg g$^{-1}$) can be determined (Carmona et al., 2008; Perrin et al., 2015).

## 2.4 | Proteomics analysis

The midbrain blocks were sampled before mass spectrometry runs as follows: midbrain sample blocks were transferred to a cryostat chamber at −20°C and kept until temperature balancing. Each block was punched 4–6 times at a depth of 5 mm with a 20-G Quincke Spinal Needle (Becton Dickinson, cat. no. 405182). Whenever areas of pigmentation were visible, biopsies were taken directly from those regions. Around 20 mg of tissue was collected into reaction tubes and kept at −80°C until further use. Tissue lysis was performed in freshly prepared lysis buffer consisting of 7 M urea (Sigma-Aldrich, cat. no. U5378-500G), 2 M thiourea (Sigma-Aldrich, cat. no. T8656), 4% Chaps (Applichem, cat. no. A1099), 2% ASB14 (Sigma-Aldrich, cat. no. A1346-1G), 1:25 (v/v %) cOmplete™ mini-EDTA-free protease inhibitor (Roche, cat. no. 11836170001), and 1:20 (v/v %) PhosStop phosphatase inhibitor (Roche, cat. no. 4906845001) dissolved in deionized water. For mass spectrometry sample preparation, 50 µg protein was loaded into a 4–12% NuPAGE Novex Bis-Tris Minigel (Invitrogen, cat. no. NP0335BOX), run for 1.5 cm, and stained with Coomassie Brilliant Blue (Sigma, cat. no. 1.12553). Protein areas were cut out, diced, and subjected to reduction with dithiothreitol (Sigma-Aldrich, cat. no. D0632-10G), alkylation with iodoacetamide (Sigma-Aldrich, cat. no. I6125), and finally digested with trypsin (Sigma-Aldrich, cat. no. T1426) overnight. Tryptic peptides were extracted from the gel and the solution was dried in a Speedvac (Atanassov & Urlaub, 2013). For peptide library generation, aliquots of equal amounts from each sample were pooled to a total amount of 80 µg and further separated into eight fractions using a reversed-phase spin column (Pierce High-pH Reversed-Phase Peptide Fractionation Kit, Thermo Fisher Scientific, cat. no. 84868). All samples were spiked with a synthetic peptide standard used for retention time alignment (iRT Standard, Schlieren, Schweiz). Protein digests were analyzed on a nanoflow chromatography system (Eksigent nanoLC425) hyphenated to a hybrid triple-quadrupole TOF mass spectrometer (TripleTOF 5600+) equipped with a Nanospray III ion source (Ionspray Voltage 2400 V, Interface Heater Temperature 150°C, Sheath Gas Setting 12) and controlled by Analyst TF 1.7.1 software build 1163 (RRID:SCR_015785, all AB Sciex). In brief, peptides were dissolved in a loading buffer (2% acetonitrile, cat. no. 491683, 0.1% formic acid, cat. no. 399388, in water) to a concentration of 0.3 µg/µL. For each analysis, 1.5 µg of digested protein was enriched on a pre-column (0.18 mm ID × 20 mm, Symmetry C18, 5 µm, Waters, Milford/MA, USA, cat.

no. WAT054275) and separated on an analytical RP-C18 column (0.075 mm ID × 250 mm, HSS T3, 1.8 µm, Waters, cat. no. 186007474) using a 90 min linear gradient of 5–35% acetonitrile/0.1% formic acid (v:v) at 300 nL·min$^{-1}$. Qualitative LC/MS/MS analysis was performed using a Top25 data-dependent acquisition method with an MS survey scan of $m/z$ 350–1250 accumulated for 350 ms at a resolution of 30 000 full width at half maximum (FWHM). MS/MS scans of $m/z$ 180–1600 were accumulated for 100 ms at a resolution of 17 500 FWHM and a precursor isolation width of 0.7 FWHM, resulting in a total cycle time of 2.9 s. Precursors above a threshold MS intensity of 125 cps with charge states 2+, 3+, and 4+ were selected for MS/MS, and the dynamic exclusion time was set to 30 s. MS/MS activation was achieved by CID using nitrogen as a collision gas and the manufacturer's default rolling collision energy settings. Three technical replicates per reversed-phase fraction were analyzed to construct a spectral library. For quantitative analysis by data-independent acquisition mass spectrometry (DIA-MS), MS/MS data were acquired using 65 variable-size windows (Zhang et al., 2015) across the 400–1050 $m/z$ range. Fragments were produced using rolling collision energy settings for charge state 2+, and fragments were acquired over an $m/z$ range 350–1400 for 40 ms per segment. Including a 100 ms survey scan, this resulted in an overall cycle time of 2.75 s. Either two or three replicate injections were acquired for each biological sample. Protein identification was achieved using ProteinPilot Software version 5.0 build 4769 (RRID:SCR_018681, AB Sciex) at "thorough" settings. A total of 407 752 MS/MS spectra from the combined qualitative analyses were searched against the UniProtKB human reference proteome (revision 04–2018, 93 609 entries) augmented with a set of 52 known common laboratory contaminants to identify 2498 proteins at an FDR of 1%. Spectral library generation and DIA-MS peak extraction were achieved in PeakView Software version 2.1 build 11 041 (RRID:SCR_015786, AB Sciex) using the quantitation microApp version 2.0 build 2003. Following retention time correction using the iRT standard, peak areas were extracted using information from the MS/MS library at an FDR of 1% (Lambert et al., 2013). The resulting peak areas were then summed to peptide and, finally, protein area values. After protein quantitation and statistical analyses, differentially expressed proteins were extracted from the datasets and filtered according to a gene ontology term compilation using the online platform AmiGO2 (http://amigo.geneontology.org/; Carbon et al., 2008). Briefly, a gene ontology (GO) term search was conducted for the following main keywords: "metal homeostasis" and "metal transport," as well as for "iron," "copper," "chloride," and "potassium" (Supplementary S3). The identified GO terms were referred to throughout the manuscript as "GO terms of interest." The components of the GO terms of interest were extracted. After homogenization of the nomenclature to UNIPROT (cat. no. RRID:SCR_002380) primary accessions, the identified candidates were matched with the DE proteins identified by DIA-MS experiments (separately for the comparison of PD vs. Ctrl samples, and the comparison of MS vs. Ctrl samples). Analysis of protein–protein interaction (PPI) networks was performed using STRING (RRID:SCR_005223) version 11.0 (Szklarczyk et al., 2014) with a

minimum interaction score of 0.4 as a requirement. Pathway enrichment analysis was performed with ShinyGO (RRID:SCR_019213) v. 0.77, using standard settings (FDR cutoff = 0.05; minimum pathway size = 2; and maximum pathway size = 2000).

## 2.5 | Statistics

Statistical analyses on demographics and clinical characteristics (Supplementary S4) were performed with the software GraphPad Prism 8.0 (GraphPad Software, San Diego, USA, RRID:SCR_002798, http://www.graphpad.com/), checking normality postulates with Shapiro–Wilk's test. For "age" and "post-mortem interval" data, ANOVA one-way test and Tukey post hoc were applied to the three groups (Ctrl, MS, and PD), for "sex," the Fisher's exact test was employed, while for "disease duration," unpaired t-test was implemented.

For PIXE/RBS data, statistical analyses were performed using GraphPad Prism 8.0. No test for outliers was conducted. Non-parametric tests were used, either because a small population was involved or because normality was not fulfilled. For Figure 2 and Supplementary S5, Kruskal–Wallis test and Dunn's test for multiple comparisons were performed, independently for NM neurons and surrounding tissues. For Figure 3, principal component analysis (PCA) was performed on elemental content and corresponding plots constructed using RStudio 1.4.1717, R 4.1.0 (RRID:SCR_000432, RStudio Team, RStudio: Integrated Development Environment for

R, Boston, MA, USA) and associated packages FactoMinerR 2.4 (Lê et al., 2008), missMDA 1.18 (Josse & Husson, 2016), factoextra 1.0.7 (Alboukadel & Fabian, 2017), and tidyverse 1.3.1 (Wickham et al., 2019). The active variables for the PCA corresponded to the quantified elements P, S, Cl, K, Ca, Fe, Cu, and Zn ($n = 8$).

For proteomics data, following sample grouping and logarithmic transformation, statistical evaluation of protein quantitation and volcano plot generation was performed in the platform Perseus v1.6.6.0 (RRID:SCR_015753, MPI for Biochemistry, Martinsried; Tyanova et al., 2016). Differential expression analysis between groups was performed using a two-sided T-test with permutation-based FDR assessment (FDR 0.1, s0 = 0, 250 randomizations).

## 3 | RESULTS

### 3.1 | Demographics and clinical characteristics

Brain-bank tissue from patients with PD, patients with MS, and control subjects without indication of neurodegenerative or neuroinflammatory pathology were used. Whereas patients with PD and controls were not different regarding their mean age of death, patients with MS were, expectedly, significantly younger. Whereas in MS patients female subjects were more frequent, males were predominant in PD, reflecting the sex difference in these disorders. Disease duration was also significantly longer in MS than in
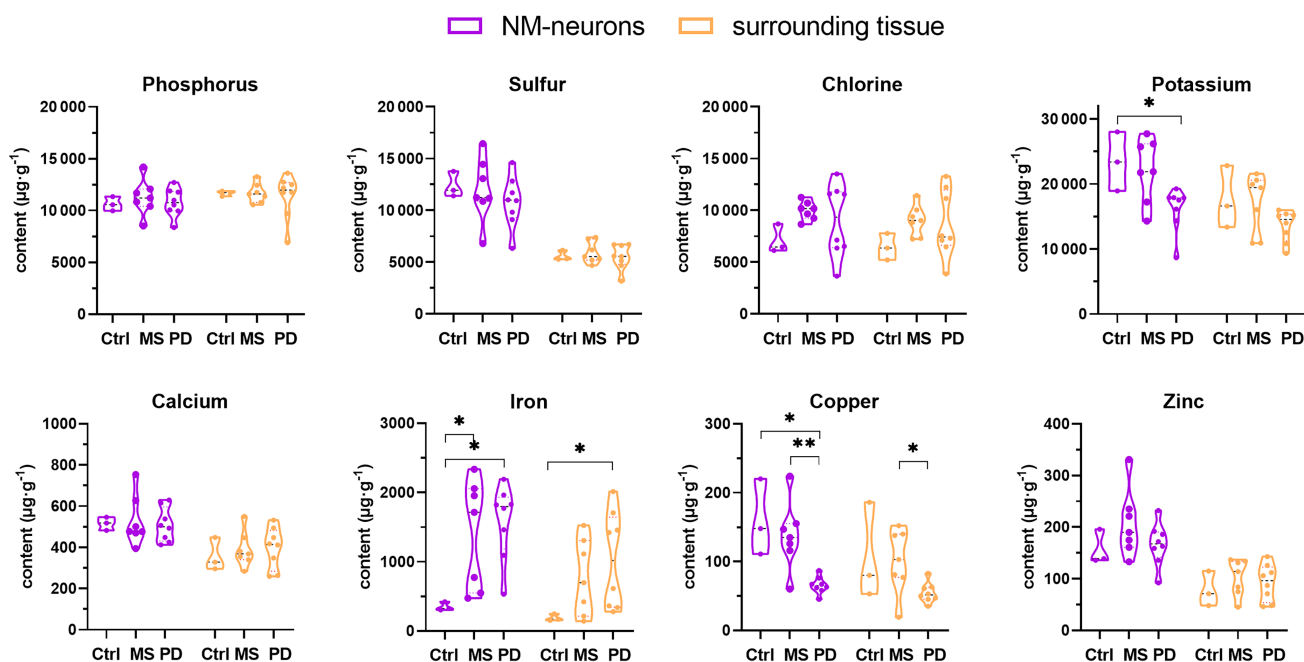


**FIGURE 2** Elemental content in neuromelanin (NM) neurons (magenta) and surrounding tissue (orange) per group. For each element, the violin plots show the median group value (black line) and the mean value of each patient (dots). Plots are truncated to the maximum and minimum values in each data group. p values were calculated by Kruskal–Wallis and Dunn's test without correction for multiple comparisons and are indicated in Supplementary S5. *$p < 0.05$, **$p < 0.01$. The number of individuals "$n$" were 3, 7, and 8 for controls (Ctrl), multiple sclerosis (MS), and Parkinson's disease (PD), respectively.
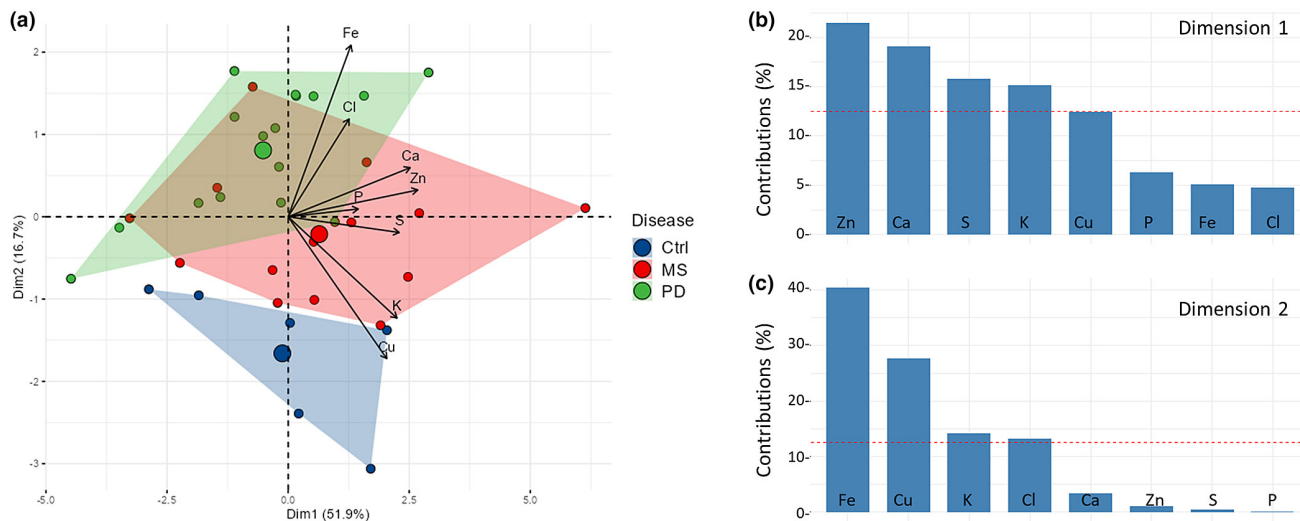
**FIGURE 3** Principal component analysis (PCA) of the elemental content in control (Ctrl), multiple sclerosis (MS), and Parkinson's disease (PD) groups. The active variables are the elemental abundancies quantified by PIXE/RBS. (a) PCA plot of Ctrl (blue), MS (red), and PD (green) across dimension 1 and dimension 2. Each circle represents one patient, including values from NM neurons and surrounding tissues, in a two-dimensional space. Larger colored circles represent the centroid for each group. The relative position of the arrows indicates the correlations between the variables and their contribution to the two dimensions. (b, c) Contribution of the different elements to the first two dimensions of the PCA expressed in %. The dotted red lines indicate the mean contribution of all the elements.

PD patients. Post-mortem intervals were not significantly different between groups (Supplementary S1 and S4).

## 3.2 | Elemental content in NM neurons and surrounding tissue

The precise tissue localization of bioelements is crucial to understand their involvement in the pathogenic process. However, most studies so far have either been performed on bulk tissue or focused on the intraneuronal content only. To better characterize the elemental distribution in the substantia nigra of brains affected by PD and MS and compare them to control tissue, we performed measurements of NM neurons and surrounding tissue. Eight chemical elements (P, S, Cl, K, Ca, Fe, Cu, and Zn) were quantified using PIXE/RBS analysis. The number of PIXE/RBS analyses per individual varied according to the number of NM neurons identified in the respective tissue section. In total, 326 measurements were performed: 165 on NM neurons and 161 on the surrounding tissue (Supplementary S2).

For each individual, we calculated the mean P, S, Cl, K, Ca, Fe, Cu, and Zn content in NM neurons and surrounding tissue (Supplementary S6). Then, we plotted the mean values for each group (Ctrl, MS, and PD) as shown in Figure 2, where each dot represents the mean value of elemental content for one patient. Statistical analysis shows that Fe content is higher in PD than in Ctrl for both NM neurons and surrounding tissue. In MS, the same trend was found except that a statistically significant difference versus Ctrl was observed only for NM neurons. Interestingly, Cu content in NM neurons is lower in PD compared to Ctrl, and also compared to

MS. Cu content remains the same in MS and Ctrl. Finally, K content is lower in NM neurons in PD compared to Ctrl. Detailed statistical results and exact p-values are presented in Supplementary S5.

To determine whether the disease groups can be differentiated by their elemental content, we performed a PCA where the active variables are all the elemental contents quantified by PIXE/RBS, which includes NM neurons and surrounding tissue values (Figure 3). The PCA clearly differentiated the control group from the PD and MS groups in the second dimension (Figure 3a), with Fe and Cu contents accounting for 40% and 27% of the contribution to dimension 2, respectively (Figure 3c). The difference with the control group is more pronounced for the PD group than for the MS group as the PD group has higher Fe values and lower Cu values than the MS group.

Fe and Cu content in NM neurons and surrounding tissue for each individual are presented in Figure 4. It is interesting to note that low Cu content is measured for all eight PD cases, both in NM neurons and surrounding tissue, while high Fe content is not systematically observed, some PD and MS patients show low Fe content values, similar to control values.

## 3.3 | Proteomic analysis of human midbrain samples

To investigate proteomic changes that might contribute to the dysregulation of metal homeostasis in the studied human tissue material, a proteomics analysis was performed: protein lysates were prepared from midbrain samples, and protein abundance profiling was performed by data-independent acquisition mass spectrometry (DIA-MS)
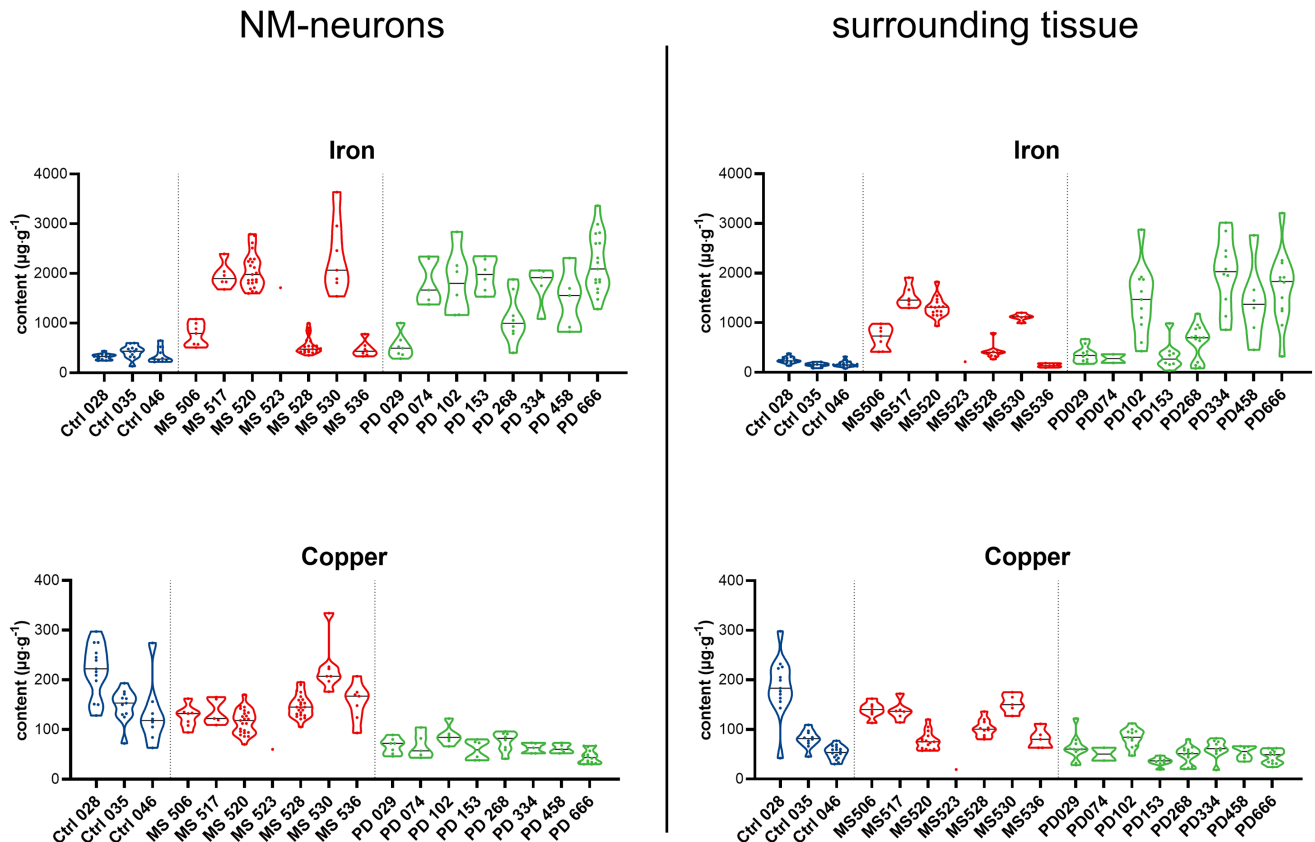
**FIGURE 4** Fe and Cu content (expressed in $\mu g\,g^{-1}$) in neuromelanin (NM) neurons and surrounding tissue for each individual. Violin plots show the median (black line) and every single measurement performed for each individual. Plots are truncated to the maximum and minimum values for each individual. Elemental content values for each analysis are presented in Supplementary S2, as well as the number "$n$" of measurements for each patient.

of the different cohorts. To improve statistical power, we included further samples for each group. These samples were not suitable for imaging because they were provided as unstructured sections from the brain bank and not available as blocks for histological analysis. In total, 2257 non-redundant protein groups were detected and quantitated across all MS runs. Sample grouping and logarithmic transformation preceded differential expression (DE) analysis. Differential protein expression results from two different comparisons (PD vs. Ctrl. / MS vs. Ctrl.) were considered for further analyses (Figure 5a,d) and functional annotation analyses were performed (Figure 5b,e). In PD samples, a pronounced enrichment for the GO terms *ferroptosis* and *endocrine regulation of calcium reabsorption* was identified, besides more general

**FIGURE 5** Proteomic analysis of human midbrain samples. (a) Volcano plot showing differential abundance of all proteins identified by data-independent acquisition mass spectrometry (DIA-MS) (for the comparison of PD vs. Ctrl samples). Differentially expressed (DE) proteins are shown in colors: 245 up-regulated proteins in PD (red); and 62 down-regulated proteins in PD (blue). DE analyses considered two-sided t-test with permutation-based FDR assessment (FDR 0.05, s0=0). (b) Functional enrichment results for DE proteins (PD vs. Ctrl). Top 15 enriched pathways are displayed. (c) Venn diagram showing the overlap between the components of gene ontology (GO) terms related to metal homeostasis and the coding genes for the identified DE proteins in PD; 33 overlapping proteins were identified, 30 of which were up-regulated. (d) Volcano plot showing differential abundance of all proteins identified by DIA-MS (for the comparison of MS vs. Ctrl samples). DE proteins are shown in colors: 132 up-regulated proteins in MS (red) and 9 down-regulated proteins in MS (blue). DE analyses considered two-sided t-test with permutation-based false discovery rate (FDR) assessment (FDR 0.05, s0=0). (e) Functional enrichment results for DE proteins (MS vs. Ctrl). Top 15 enriched pathways are displayed. (f) Venn diagram showing the overlap between the components of GO terms related to metal homeostasis and the coding genes for the identified DE proteins in MS; 12 overlapping proteins were identified, 11 of which were up-regulated. (g) Protein–protein interaction (PPI) analysis showing protein networks for the 33 candidates of interest identified for PD (DE proteins in PD that overlapped with candidates involved in metal homeostasis). All highlighted proteins were found up-regulated in PD. Clusters of interest are highlighted in colors (Fe homeostasis/transport; response to Cu ion; and response to K homeostasis). (h) PPI analysis showing protein networks for the 12 candidates of interest identified for MS (DE proteins in MS that overlapped with candidates involved in metal homeostasis). Except for ATP6AP1, all highlighted proteins were found up-regulated in MS. Clusters of interest are highlighted in colors (cellular metal-ion homeostasis; response to metal ion). (i) Heatmap showing the mean expression of selected DE proteins involved in metal homeostasis in PD, MS, and Ctrl conditions. Demographic data for the proteomic analysis are presented in Supplementary S4.
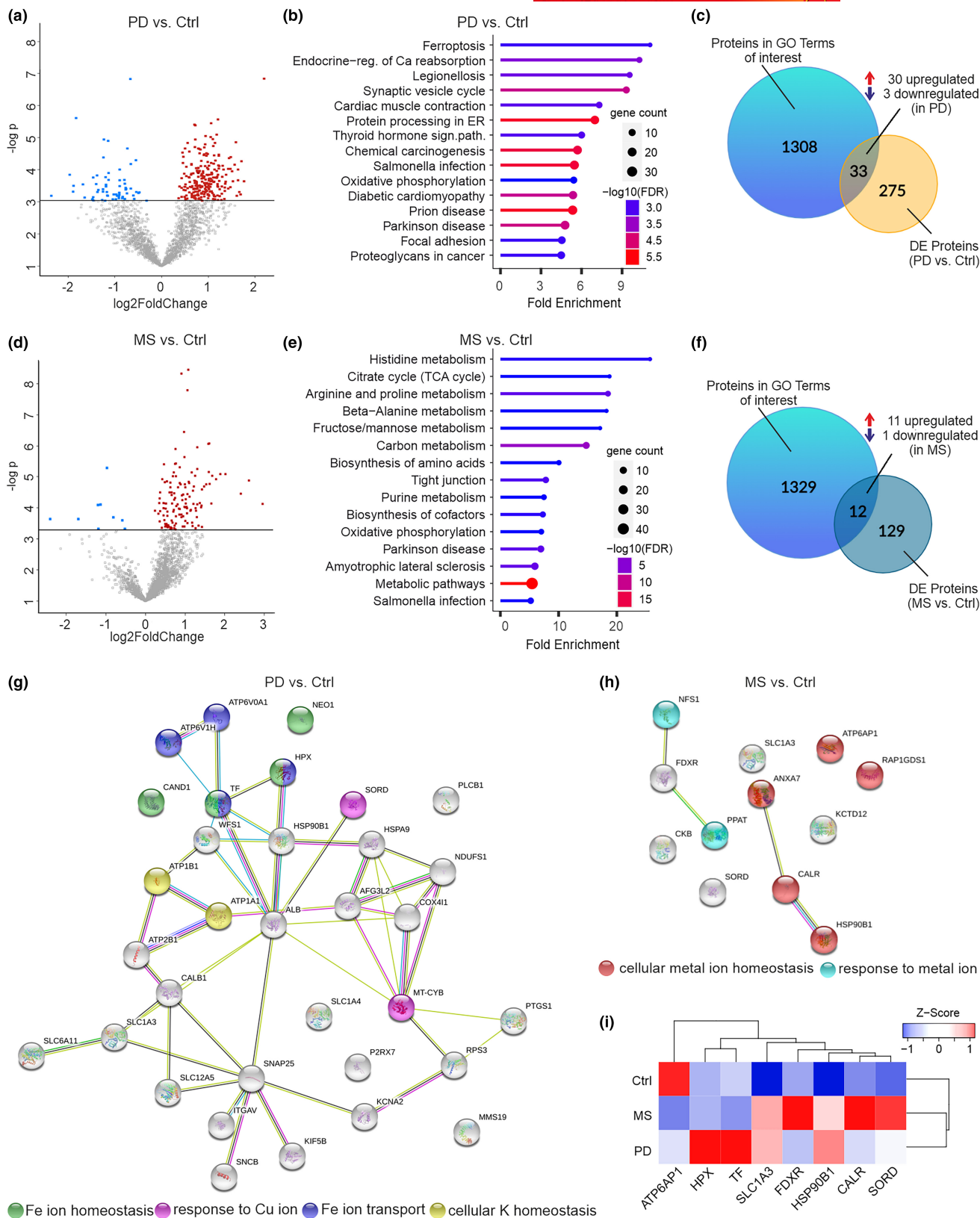
pathways related to neurodegeneration, immune system activation, and general metabolism were identified for both PD and MS cohorts.

Next, the DE results were filtered according to a GO term compilation. Briefly, this step was based on compiling coding genes/protein candidates which belong to GO terms related to general metabolism processes, and also terms related to specific elements of interest for this work. A list of the GO terms of interest that were identified during the data retrieval

**136** | **WILEY**—Journal of Neurochemistry | JNC The Official Journal of the International Society for Neurochemistry

CARMONA ET AL.

is provided as a Supplementary S3 table. A final list of unique candidates related to GO terms of interest comprised a total of 1341 entities. Proteins that overlapped the lists of the GO term compilation and the proteomics differential expression results (Figure 5c,f) were considered for PPI analyses (33 proteins for the PD vs. Ctrl comparison; 12 proteins for the MS vs. Ctrl comparison) (Supplementary S7). In both comparisons, the vast majority of the DE proteins presented a significant up-regulation in the disease state in comparison to the control patients. In order to explore PPI networks and the possible roles of the regulated candidates in biological processes related to metal homeostasis, STRING analyses were conducted with the overlapping candidates found after the GO term compilation steps (DE proteins that overlapped with candidates involved in metal homeostasis; Figure 5g,h). These analyses were conducted separately for each comparison. For the PD versus Ctrl. comparison, a cluster associated with Fe homeostasis and Fe transport is highlighted. All of the proteins in that cluster are found up-regulated in PD patients. Important hub proteins were depicted, including Fe-interacting proteins such as hemopexin (HPX) and transferrin (TF). Furthermore, proteins associated with response to Cu-ion and cellular potassium homeostasis are found in the differential protein list. Likewise, all of those proteins are found up-regulated in PD. The comparison between MS and Ctrl identified proteins related to cellular metal-ion homeostasis and response to metal ions. All proteins except one (ATP6AP1) are found up-regulated in MS patients when compared to Ctrl. Important hub proteins, calreticulin (CALR) and ferredoxin reductase (FDXR), were identified in MS. Only three proteins show regulation in both disease groups (SLC1A3, SORD, and HSP90B1).

## 4 | DISCUSSION

### 4.1 | Nigral iron dyshomeostasis in PD and MS

Since the discovery of Fe deposits in the brains of PD patients almost a century ago (Lhermitte et al., 1924), numerous studies have been conducted to explain this observation. This increased Fe content in the brains of PD patients has been confirmed and particularly localized to the degenerating SN pars compacta (Dexter et al., 1989; Hirsch et al., 1991; Ward et al., 2014). Other studies have also found that Fe content was increased in NM neurons of PD patients compared to NM neurons from control individuals using analytical methods with high-spatial-resolution capabilities (Davies et al., 2014; Friedrich et al., 2021; Oakley et al., 2007). High Fe content is not limited to the NM neurons, the increase in Fe is also observed in astrocytes, macrophages, reactive microglia, and non-pigmented neurons as well as in affected areas devoid of pigmented neurons in the SN of PD patients (Jellinger et al., 1990). A more recent study has identified increased Fe levels in microglial and oligodendroglial cells, but not in astrocytes (Friedrich et al., 2021). Moreover, PD patients show

elevated Fe levels both in the NM neurons and immediately adjacent surrounding tissue (Oakley et al., 2007). Interestingly, iron interacts with alpha-synuclein (reviewed in Lingor et al., 2017; Joppe et al., 2019) and an increase in brain iron alters alpha-synuclein aggregation (Dauer Née Joppe et al., 2021). There is thus compelling evidence of Fe accumulation in the SN of PD patients, and this excess Fe can be visualized using magnetic resonance imaging (MRI) (Li et al., 2022). Recently, we also shown that longitudinal quantification of Fe and ferritin in CSF could reflect disease progression in PD and thus may represent an auspicious biomarker (Maass et al., 2021). Whether this iron accumulation is contributing to the progression of neurodegeneration in PD is still debated. A recent trial of deferiprone in patients with PD (FAIR-PARK) failed to show beneficial effects of iron chelation on disease progression (Devos et al., 2022). Some studies do not report differences between Fe in the SN from PD patients and controls (Friedman & Galazka-Friedman, 2012; Loeffler et al., 1995; Scholefield et al., 2021; Uitti et al., 1989).

In our study, we measured a 4.5- and 2.9-fold increase in nigral iron in PD compared with controls, in NM neurons, and surrounding tissue, respectively (Figure 2). Previous studies have shown that Fe content increases with age in the SN of healthy subjects, with a difference of around 15% between individuals aged 65 and those aged 78.5 (Zecca, Stroppolo, et al., 2004). The very high increase in nigral Fe that we measured cannot therefore be attributed to the age difference between the groups of control subjects (65 years on average) and PD patients (78.5 years). Our study thus confirms existing observations showing increased Fe deposition in the SN of PD at the tissue level (Ayton et al., 2013; Dexter et al., 1989; Genoud et al., 2017; Hirsch et al., 1991; Jellinger et al., 1990; Lhermitte et al., 1924; Ward et al., 2014). Our results also confirm that Fe content is higher in NM neurons from PD patients versus controls at the single neuron level (Davies et al., 2014; Friedrich et al., 2021; Oakley et al., 2007). We also show that Fe accumulation is not limited to NM neurons but extends to the entire surrounding tissue, suggesting a general increase in Fe in the SN of PD patients. In addition, our study indicates that high nigral Fe is not systematically observed among PD patients (Figure 4). This variability may explain why high Fe content in the SN of PD brains is not evidenced in all studies (Uitti et al., 1989; Loeffler et al., 1995; Scholefield et al., 2021) and why iron chelation therapy using deferiprone may have failed in an unselected patient population (Devos et al., 2022). This fact differs greatly from the systematic decrease in Cu found in this brain region in PD patients (see further discussion on Cu dyshomeostasis). As shown by our work and that published by other teams, the variability of Fe content in the SN of PD patients argues for targeted therapeutic intervention by iron chelation therapy only for those patients for whom iron overload in the SN would be diagnosed by MRI.

In MS, numerous studies have evidenced Fe dyshomeostasis in the brain, showing Fe accumulation in the gray matter and Fe depletion in the normal-appearing white matter (reviewed in Stephenson et al., 2014; Dales & Desplat-Jégo, 2020). MRI shows

Fe accumulation in the deep gray matter of MS patients (reviewed in Khalil et al., 2011; Stankiewicz et al., 2014). Histological studies on MS brains revealed that Fe was low in normal-appearing white matter, probably as a result of the loss of Fe-rich oligodendrocytes, while Fe accumulated at the edges of chronic MS lesions where Fe was located mainly in macrophages (Hametner et al., 2013). Another study, using synchrotron X-ray fluorescence quantitative metal imaging, indicated that Fe did not accumulate in chronic MS lesions but rather in a subset of chronic inactive lesions (Popescu et al., 2017). The relationship between Fe and MS has been extensively studied in various brain regions but not in the SN, with only one existing report (Blazejewska et al., 2015). In contrast to PD, neurodegeneration likely occurs as a secondary mechanism in MS, and less is known about the role of iron in this autoimmune disorder. We measured a significant increase in Fe content in NM neurons from MS patients compared to controls (Figure 2). There is also an increase in Fe content in the surrounding tissue, although the result was not statistically significant. Our results are in agreement with the increased Fe content in the SN in patients with relapsing–remitting MS compared with healthy controls, as observed by MRI (Blazejewska et al., 2015). This result suggests that Fe accumulation in NM neurons does not necessarily result in degeneration of NM neurons and PD symptoms, but may represent a general signature of neurodegeneration, which was not observed in control subjects. In line with this, analysis of nationwide registry data from Denmark shows no increased risk of PD in MS patients (Nielsen et al., 2014).

## 4.2 | Nigral copper dyshomeostasis in PD

Although Fe dyshomeostasis has been extensively investigated, fewer studies have addressed so far the question of Cu dyshomeostasis in PD (reviewed in Abdeen et al., 2022). We observed a statistically significant 2.4-fold (59%) decrease in Cu content in PD NM neurons versus control neurons, and a similar 2.1-fold decrease when comparing Cu in NM neurons from PD patients to those with MS (Figure 2). This result is in agreement with published data showing a large deficit of nigral Cu content in PD patients when compared to age-matched controls (Ayton et al., 2013; Davies et al., 2014; Dexter et al., 1989; Genoud et al., 2017; Scholefield et al., 2021; Uitti et al., 1989). Early studies indicated a 25–45% reduction in total Cu content in the SN of patients with PD (Dexter et al., 1989; Uitti et al., 1989). More recently, NM-associated Cu and Cu transport protein 1 (CTR1) was shown to be significantly reduced in the SN of PD with 45% and 50% decrease, respectively (Davies et al., 2014). In this same study, a 48% decrease in NM-associated Cu was also observed in incidental Lewy body disease (ILBD) patients compared to age-matched control subjects. These results suggest a potential link between Cu deficit and the vulnerability of the SN not only in PD but also in ILBD, a pathology suggested to represent pre-clinical PD (Dickson et al., 2009). Since Cu deficit occurred in ILBD, with limited cell loss in the SN, the authors suggested that early deficit may precede cell death and

clinical symptoms (Davies et al., 2014). In another study, a decrease of about 50% in Cu total concentrations was reported in the SN from PD patients compared to age-matched controls, and this Cu decrease originated in the soluble cellular fraction rather than the membrane-associated or insoluble fractions (Genoud et al., 2017). In a recent study of the multi-elemental composition of PD brains, Cu concentrations were the most consistently perturbed, with a 34% decrease in the SN (Scholefield et al., 2021). Compared to previous studies, our results provide several novel aspects. First, local quantification of Cu content determined that the global Cu deficit previously reported for the SN of PD patients is as a result of a decrease in Cu in NM neurons and probably to a similar decrease in the surrounding tissue, although the difference is not statistically significant compared to controls, but it is in relation to MS patients. In contrast to the heterogeneity of Fe in the SN of PD patients, our results further indicate that Cu deficiency in NM neurons is much more homogeneous in all measured PD patients (Figure 4), and never observed in MS patients. It is well documented that demyelinating lesions also occur in the substantia nigra of MS patients (Chen et al., 2012; Vercellino et al., 2009; Walter et al., 2009). Therefore, our results suggest that Cu depletion in the SN may be a more specific hallmark of PD, while increased iron levels reflect neurodegeneration in general. While the increase in nigral Fe content could be mainly attributed to an increase in Fe storage proteins, such as ferritin, and this storage can be exceeded in the context of disease, the problem could be more complex in the case of Cu depletion, which would affect the function of a large number of proteins such as Cu, Zn superoxide dismutase, cytochrome c oxidase, and many others. Copper-containing compounds, such as CuII(ATSM), a bis-(thiosemicarbazone) derivative, have been identified as potential drugs for the treatment of PD showing promising results in animal models (Cheng et al., 2016; Hung et al., 2012).

## 4.3 | Nigral potassium dyshomeostasis in PD

Our study also revealed that K content is significantly reduced by a factor of 1.4 in NM neurons from patients with PD (Figure 2). K depletion is not observed in the SN NM neurons of MS patients, which are not affected by the neurodegenerative process. Tight regulation of potassium homeostasis is important for cell viability. During apoptosis, K channels are up-regulated resulting in excessive K efflux and intracellular K depletion (Yu, 2003). Dysfunction of potassium channels has been involved in the etiology of PD (reviewed in Zhang et al., 2020). The increase in potassium channels may exacerbate cell damage linking K efflux to neurodegeneration. Our data on K depletion in NM neurons could reflect impaired neuronal viability in PD. Only one other study has addressed the question of K levels in the SN of PD patients compared to healthy controls, however, showing no difference between groups (Scholefield et al., 2021). In contrast, our study differentiates between intra- and extra-neuronal K and therefore yields a more

precise representation than a bulk quantification of the whole SN tissue.

## 4.4 | Proteomics changes related to metal homeostasis in PD and MS

The analysis of proteomics data revealed an up-regulation of many proteins in the SN of both PD and MS samples compared to controls (Figure 5a). These findings are in line with a meta-analysis that reported a transcriptomic up-regulation in the SN in PD (Mariani et al., 2016). Since this study revealed significant differences in metal content, we further explored the proteomics results for gene ontology terms related to metal homeostasis. Overall, the number of deregulated proteins that are associated with metal homeostasis was much larger in PD than in MS (Figure 5c,f). This goes in line with disease characteristics since the midbrain SN is the most affected region in PD-affected brains, especially at late stages. In contrast to PD, the midbrain is usually spared from obvious pathology in MS although demyelinating lesions are also known to affect the SN of MS patients (Chen et al., 2012; Vercellino et al., 2009; Walter et al., 2009). Moreover, the number of deregulated proteins that are associated with metal homeostasis was also much larger in PD than in MS. This is in agreement with the PIXE results indicating that a more prominent dysbalance in metal homeostasis is present in PD when compared to MS. These findings are likely associated with the more prominent neurodegenerative events that occur in the midbrain of advanced-stage PD patients (Dexter et al., 1989; Hirsch et al., 1991; Ward et al., 2014). Furthermore, the proteomics data highlight an important cluster associated with Fe homeostasis and Fe transport in PD, in line with both the results for a Fe enrichment in SN in PD described here, as well as with several studies in the field (Jellinger, 2013; Jellinger et al., 1990; Ward et al., 2014; Zecca, Youdim, et al., 2004). Interestingly, among the up-regulated candidates, we identified major Fe-interacting proteins. These included hemopexin (HPX), a Heme-binding protein widely present in blood that has neuroprotective potential by regulating Fe levels in inflammatory states, for example, after traumatic brain injury (Delanghe & Langlois, 2001; Hahl et al., 2013). Another candidate was transferrin (TF), an iron delivery protein that is pivotal for Fe homeostasis in the brain (Leitner & Connor, 2012). The up-regulation of such candidates might reflect the presence of compensatory mechanisms related to the increased Fe levels in PD brains. On the other hand, the dysbalance in such protein levels might also directly contribute to disease mechanisms of PD. Studying iron chelators (Perez et al., 2008) may thus be an auspicious strategy to explore the importance of these alterations for PD pathology.

For MS samples, changes in the expression of proteins related to metal homeostasis seemed more general, with fewer networks and hub proteins involved. Clusters related to *cellular metal ion homeostasis* and *response to metal ion* appeared in PPI network analyses for MS results, with the most prominent hub protein being calreticulin (CALR). This soluble chaperone is known to bind Ca and Zn

with high affinity and was shown to increase after stress induction, as well as in the presence of heavy metals in vitro (Li et al., 2001; Nguyen et al., 1996). Interestingly, only three proteins have shown a similar regulation in both PD and MS groups (SLC1A3, SORD, and HSP90B1). Overall, the proteomics findings suggest that metal dysbalance is equally reflected on the proteomic level, is more pronounced in PD than MS, and likely involves different mechanisms in both disorders.

## 5 | CONCLUSIONS

Our study enabled us to identify and compare characteristic features of metal dyshomeostasis in PD and MS. Obtaining valuable frozen post-mortem specimens allowed us to reliably study metal homeostasis without changes in their native content and distribution known to occur in chemically stored/treated samples. This relatively large number of rare frozen human brain specimens has enabled us to identify statistically significant differences in metal content. Using high-resolution chemical element imaging, we show that variations in intraneuronal metal concentrations are generally accompanied by the same modifications in the extra-neuronal tissue. We confirm the increase in Fe in the SN from PD compared to healthy individuals but also point out the variability of nigral Fe content among PD patients arguing for individualized therapeutic approaches. Increased Fe in NM neurons is also observed in MS patients showing no PD symptoms, indicating that this parameter alone is not sufficient to explain dopaminergic neuron dysfunction. Our data confirm that Fe overload in the CNS is a general trait encountered in many neurodegenerative diseases. In contrast, MS and PD are characterized by very different trends for Cu quantitative distribution. Low Cu in PD NM neurons and the surrounding tissue compared to controls is a parameter observed systematically for PD cases but not observed in MS. Potassium is also decreased in PD NM neurons and not in MS. Both Cu and K decrease in the NM neurons from SN are characteristic features of PD. Using PCA, we highlighted that Fe and Cu levels in the SN could differentiate disease groups from healthy individuals. Proteomics analyses on the same samples could hint toward disease mechanisms in PD and MS, highlighting important PPI networks associated with Fe homeostasis and Fe transport in PD. For MS, changes in the expression of proteins related to metal homeostasis are more general. Overall, proteomics data and metal quantitative imaging suggest that metal dyshomeostasis in PD patients involves other mechanisms than in patients with MS.

### AUTHOR CONTRIBUTIONS

**Asuncion Carmona:** Data curation; formal analysis; writing – original draft; writing – review and editing; conceptualization; methodology. **Eleonora Carboni:** Data curation; formal analysis; writing – review and editing; methodology. **Lucas Caldi Gomes:** Formal analysis; writing – review and editing; writing – original draft; methodology; data curation. **Stéphane Roudeau:** Formal analysis; writing – review and

## CONFLICT OF INTEREST STATEMENT

The authors declare that they have no known competing financial interests or personal relationships that could have appeared to influence the work reported in this paper.

## PEER REVIEW

The peer review history for this article is available at https://www.webofscience.com/api/gateway/wos/peer-review/10.1111/jnc.16040.

## DATA AVAILABILITY STATEMENT

All individual data on chemical element quantitative analysis are available in the Supplementary Material. Other data will be available on request.

## ORCID

*Asuncion Carmona* https://orcid.org/0000-0002-9253-4581
*Eleonora Carboni* https://orcid.org/0000-0003-1354-1239
*Lucas Caldi Gomes* https://orcid.org/0000-0003-4959-2169
*Stéphane Roudeau* https://orcid.org/0000-0002-4539-9380
*Fabian Maass* https://orcid.org/0000-0002-4077-2852
*Christof Lenz* https://orcid.org/0000-0002-0946-8166
*Richard Ortega* https://orcid.org/0000-0003-1692-5406
*Paul Lingor* https://orcid.org/0000-0001-9362-7096

## REFERENCES

Abdeen, A. H., Trist, B. G., & Double, K. L. (2022). Empirical evidence for biometal dysregulation in Parkinson's disease from a systematic review and Bradford Hill analysis. *NPJ Parkinsons Disease*, 8(1), 83.

Acevedo, K., Masaldan, S., Opazo, C. M., & Bush, A. I. (2019). Redox active metals in neurodegenerative diseases. *Journal of Biological Inorganic Chemistry*, 24(8), 1141–1157.

Alboukadel, K., & Fabian, M. (2017). *Factoextra: Extract and visualize the results of multivariate data analyses*. R package version 1.0.5., https://CRAN.R-project.org/package=factoextra

Atanassov, I., & Urlaub, H. (2013). Increased proteome coverage by combining PAGE and peptide isoelectric focusing: Comparative study of gel-based separation approaches. *Proteomics*, 13, 2947–2955.

Ayton, S., Lei, P., Duce, J. A., Wong, B. X., Sedjahtera, A., Adlard, P. A., Bush, A. I., & Finkelstein, D. I. (2013). Ceruloplasmin dysfunction and therapeutic potential for Parkinson disease. *Annals of Neurology*, 73(4), 554–559.

Barnham, K. J., & Bush, A. I. (2014). Biological metals and metal-targeting compounds in major neurodegenerative diseases. *Chemical Society Reviews*, 43(19), 6727–6749.

Biesemeier, A., Eibl, O., Eswara, S., Audinot, J. N., Wirtz, T., Pezzoli, G., Zucca, F. A., Zecca, L., & Schraermeyer, U. (2016). Elemental mapping of Neuromelanin organelles of human substantia Nigra: Correlative ultrastructural and chemical analysis by analytical transmission electron microscopy and nano-secondary ion mass spectrometry. *Journal of Neurochemistry*, 138(2), 339–353.

Blazejewska, A. I., Al-Radaideh, A. M., Wharton, S., Lim, S. Y., Bowtell, R. W., Constantinescu, C. S., & Gowland, P. A. (2015). Increase in the iron content of the substantia nigra and red nucleus in multiple sclerosis and clinically isolated syndrome: A 7 tesla MRI study. *Journal of Magnetic Resonance Imaging*, 41(4), 1065–1070.

Campbell, J. L., Boyd, N. I., Grassi, N., Bonnick, P., & Maxwell, J. A. (2010). The Guelph PIXE Software Package IV. *Nuclear Instruments and Methods in Physics B*, 268, 3356–3363.

Carbon, S., Ireland, A., Mungall, C. J., Shu, S., Marshall, B., Lewis, S., AmiGO Hub; Web Presence Working Group. (2008). AmiGO: Online access to ontology and annotation data. *Bioinformatics*, 25(2), 288–289.

Carmona, A., Devès, G., & Ortega, R. (2008). Quantitative micro-analysis of metal ions in subcellular compartments of cultured dopaminergic cells by combination of three ion beam techniques. *Analytical and Bioanalytical Chemistry*, 390, 1585–1594.

Carmona, A., Roudeau, S., Perrin, L., Carcenac, C., Vantelon, D., Savasta, M., & Ortega, R. (2019). Mapping chemical elements and iron oxidation states in the substantia nigra of 6-hydroxydopamine lesioned rats using correlative immunohistochemistry with proton and synchrotron micro-analysis. *Frontiers in Neuroscience*, 13, 1014.

Chen, S., Lu, F. F., Seeman, P., & Liu, F. (2012). Quantitative proteomic analysis of human substantia nigra in Alzheimer's disease, Huntington's disease and multiple sclerosis. *Neurochemical Research*, 37(12), 2805–2813.

Cheng, L., Quek, C. Y., Hung, L. W., Sharples, R. A., Sherratt, N. A., Barnham, K. J., & Hill, A. F. (2016). Gene dysregulation is restored in the Parkinson's disease MPTP neurotoxic mice model upon treatment of the therapeutic drug Cu(II)(atsm). *Scientific Reports*, 6, 22398.

Dales, J. P., & Desplat-Jégo, S. (2020). Metal imbalance in neurodegenerative diseases with a specific concern to the brain of multiple sclerosis patients. *International Journal of Molecular Sciences*, 21(23), 9105.

Dauer Née Joppe, K., Tatenhorst, L., Caldi Gomes, L., Zhang, S., Parvaz, M., Carboni, E., Roser, A. E., El DeBakey, H., Bähr, M., Vogel-Mikuš, K., Wang Ip, C., Becker, S., Zweckstetter, M., & Lingor, P. (2021). Brain iron enrichment attenuates α-synuclein spreading after injection of preformed fibrils. *Journal of Neurochemistry*, 159(3), 554–573.

Davies, K. M., Bohic, S., Carmona, A., Ortega, R., Cottam, V., Hare, D. J., Finberg, J. P., Reyes, S., Halliday, G. M., Mercer, J. F., & Double, K. L. (2014). Copper pathology in vulnerable brain regions in Parkinson's disease. *Neurobiology of Aging*, 35(4), 858–866.

Delanghe, J. R., & Langlois, M. R. (2001). Hemopexin: A review of biological aspects and the role in laboratory medicine. *Clinica Chimica Acta*, 312(1–2), 13–23.

Devos, D., Labreuche, J., Rascol, O., Corvol, J. C., Duhamel, A., … FAIRPARK-II Study Group. (2022). Trial of Deferiprone in

Parkinson's disease. *The New England Journal of Medicine, 387*(22), 2045–2055.

Dexter, D. T., Wells, F. R., Lees, A. J., Agid, F., Agid, Y., Jenner, P., & Marsden, C. D. (1989). Increased nigral iron content and alterations in other metal ions occurring in brain in Parkinson's disease. *Journal of Neurochemistry, 52*(6), 1830–1836.

Dickson, D. W., Braak, H., Duda, J. E., Duyckaerts, C., Gasser, T., Halliday, G. M., Hardy, J., Leverenz, J. B., Del Tredici, K., Wszolek, Z. K., & Litvan, I. (2009). Neuropathological assessment of Parkinson's disease: Refining the diagnostic criteria. *Lancet Neurology, 8*, 1150–1157.

Friedman, A., & Galazka-Friedman, J. (2012). The history of the research of iron in parkinsonian substantia nigra. *Journal of Neural Transmission (Vienna), 119*(12), 1507–1510.

Friedrich, I., Reimann, K., Jankuhn, S., Kirilina, E., Stieler, J., Sonntag, M., Meijer, J., Weiskopf, N., Reinert, T., Arendt, T., & Morawski, M. (2021). Cell specific quantitative iron mapping on brain slices by immuno-μPIXE in healthy elderly and Parkinson's disease. *Acta Neuropathologica Communications, 9*(1), 47.

Genoud, S., Roberts, B. R., Gunn, A. P., Halliday, G. M., Lewis, S. J. G., Ball, H. J., Hare, D. J., & Double, K. L. (2017). Subcellular compartmentalisation of copper, iron, manganese, and zinc in the Parkinson's disease brain. *Metallomics, 9*(10), 1447–1455.

Greenough, M. A., Ramírez Munoz, A., Bush, A. I., & Opazo, C. M. (2016). Metallo-pathways to Alzheimer's disease: Lessons from genetic disorders of copper trafficking. *Metallomics, 8*(9), 831–839. https://doi.org/10.1039/c6mt00095a

Hahl, P., Davis, T., Washburn, C., Rogers, J. T., & Smith, A. (2013). Mechanisms of neuroprotection by hemopexin: Modeling the control of heme and iron homeostasis in brain neurons in inflammatory states. *Journal of Neurochemistry, 125*(1), 89–101.

Hametner, S., Wimmer, I., Haider, L., Pfeifenbring, S., Brück, W., & Lassmann, H. (2013). Iron and neurodegeneration in the multiple sclerosis brain. *Annals of Neurology, 74*(6), 848–861.

Hirsch, E. C., Brandel, J. P., Galle, P., Javoy-Agid, F., & Agid, Y. (1991). Iron and aluminum increase in the substantia nigra of patients with Parkinson's disease: An X-ray microanalysis. *Journal of Neurochemistry, 56*(2), 446–451.

Hung, L. W., Villemagne, V. L., Cheng, L., Sherratt, N. A., Ayton, S., White, A. R., Crouch, P. J., Lim, S., Leong, S. L., Wilkins, S., George, J., Roberts, B. R., Pham, C. L., Liu, X., Chiu, F. C., Shackleford, D. M., Powell, A. K., Masters, C. L., Bush, A. I., ... Barnham, K. J. (2012). The hypoxia imaging agent CuII(atsm) is neuroprotective and improves motor and cognitive functions in multiple animal models of Parkinson's disease. *The Journal of Experimental Medicine, 209*(4), 837–854.

Jellinger, K., Paulus, W., Grundke-Iqbal, I., Riederer, P., & Youdim, M. B. (1990). Brain iron and ferritin in Parkinson's and Alzheimer's diseases. *Journal of Neural Transmission. Parkinson's Disease and Dementia Section, 2*(4), 327–340.

Jellinger, K. A. (2013). The relevance of metals in the pathophysiology of neurodegeneration, pathological considerations. *International Review of Neurobiology, 110*, 1–47.

Joppe, K., Roser, A. E., Maass, F., & Lingor, P. (2019). The contribution of iron to protein aggregation disorders in the central nervous system. *Frontiers in Neuroscience, 13*, 15.

Josse, J., & Husson, F. (2016). missMDA: A package for handling missing values in multivariate data analysis. *Journal of Statistical Software, 70*, 1–31.

Khalil, M., Teunissen, C., & Langkammer, C. (2011). Iron and neurodegeneration in multiple sclerosis. *Multiple Sclerosis International, 2011*, 606807.

Lambert, J. P., Ivosev, G., Couzens, A. L., Larsen, B., Taipale, M., Lin, Z. Y., Zhong, Q., Lindquist, S., Vidal, M., Aebersold, R., & Pawson, T. (2013). Mapping differential interactomes by affinity purification coupled with data-independent mass spectrometry acquisition. *Nature Methods, 10*(12), 1239–1245.

Lê, S., Josse, J., & Husson, F. (2008). FactoMineR: An R package for multivariate analysis. *Journal of Statistical Software, 25*, 1–18.

Leitner, D. F., & Connor, J. R. (2012). Functional roles of transferrin in the brain. *Biochimica et Biophysica Acta (BBA) - General Subjects, 1820*(3), 393–402.

Lhermitte, J., Kraus, W. M., & McAlpine, D. (1924). On the occurrence of abnormal deposits of iron in the brain in parkinsonism with special reference to its localization. *Journal of Neurology and Psychopathology, 5*(19), 195–208.

Li, K. R., Avecillas-Chasin, J., Nguyen, T. D., Gillen, K. M., Dimov, A., Chang, E., Skudin, C., Kopell, B. H., Wang, Y., & Shtilbans, A. (2022). Quantitative evaluation of brain iron accumulation in different stages of Parkinson's disease. *Journal of Neuroimaging, 32*(2), 363–371.

Li, Z., Stafford, W. F., & Bouvier, M. (2001). The metal ion binding properties of calreticulin modulate its conformational flexibility and thermal stability. *Biochemistry, 40*(37), 11193–11201.

Lingor, P., Carboni, E., & Koch, J. C. (2017). Alpha-synuclein and iron: Two keys unlocking Parkinson's disease. *Journal of Neural Transmission (Vienna), 124*(8), 973–981.

Loeffler, D. A., Connor, J. R., Juneau, P. L., Snyder, B. S., Kanaley, L., DeMaggio, A. J., Nguyen, H., Brickman, C. M., & LeWitt, P. A. (1995). Transferrin and iron in normal, Alzheimer's disease, and Parkinson's disease brain regions. *Journal of Neurochemistry, 65*(2), 710–724.

Maass, F., Michalke, B., Willkommen, D., Canaslan, S., Schmitz, M., Bähr, M., Zerr, I., & Lingor, P. (2021). Cerebrospinal fluid iron-ferritin ratio as a potential progression marker for Parkinson's disease. *Movement Disorders, 36*(12), 2967–2969.

Mariani, E., Frabetti, F., Tarozzi, A., Pelleri, M. C., Pizzetti, F., & Casadei, R. (2016). Meta-analysis of Parkinson's disease transcriptome data using TRAM software: Whole substantia Nigra tissue and single dopamine neuron differential gene expression. *PLoS One, 11*(9), e0161567.

Mayer, M. (1997). *SIMNRA User's guide, report IPP 9/113, Max-Planck-Institut fur Plasmaphysik, Garching, Germany.* http://home.mpcdf.mpg.de/~mam/Report%20IPP%209-113.pdf

Menezes Lyra da Cunha, M., Trepout, S., Messaoudi, C., Wu, T.-D., Ortega, R., Guerquin-Kern, J.-L., & Marco, S. (2016). Overview of chemical imaging methods to address biological questions. *Micron, 84*, 23–36.

Mezzaroba, L., Alfieri, D. F., Colado Simão, A. N., & Vissoci Reiche, E. M. (2019). The role of zinc, copper, manganese and iron in neurodegenerative diseases. *Neurotoxicology, 74*, 230–241.

Ndayisaba, A., Kaindlstorfer, C., & Wenning, G. K. (2019). Iron in neurodegeneration—cause or consequence? *Frontiers in Neuroscience, 13*, 180.

Nguyen, T. Q., Capra, J. D., & Sontheimer, R. D. (1996). Calreticulin is transcriptionally upregulated by heat shock, calcium and heavy metals. *Molecular Immunology, 33*(4–5), 379–386.

Nielsen, N. M., Pasternak, B., Stenager, E., Koch-Henriksen, N., & Frisch, M. (2014). Multiple sclerosis and risk of Parkinson's disease: A Danish nationwide cohort study. *European Journal of Neurology, 21*(1), 107–111.

Oakley, A. E., Collingwood, J. F., Dobson, J., Love, G., Perrott, H. R., Edwardson, J. A., Elstner, M., & Morris, C. M. (2007). Individual dopaminergic neurons show raised iron levels in Parkinson disease. *Neurology, 68*(21), 1820–1825.

Perez, C. A., Tong, Y., & Guo, M. (2008). Iron chelators as potential therapeutic agents for Parkinson's disease. *Current Bioactive Compounds, 4*(3), 150–158.

Perrin, L., Carmona, A., Roudeau, S., & Ortega, R. (2015). Evaluation of sample preparation methods for single cell quantitative element imaging using proton or synchrotron radiation focused beams. *Journal of Analytical Atomic Spectrometry, 30*, 2525–2532.

Popescu, B. F., Frischer, J. M., Webb, S. M., Tham, M., Adiele, R. C., Robinson, C. A., Fitz-Gibbon, P. D., Weigand, S. D., Metz, I., Nehzati,

S., George, G. N., Pickering, I. J., Brück, W., Hametner, S., Lassmann, H., Parisi, J. E., Yong, G., & Lucchinetti, C. F. (2017). Pathogenic implications of distinct patterns of iron and zinc in chronic MS lesions. *Acta Neuropathologica*, *134*(1), 45–64.

Roberts, E. A., & Schilsky, M. L. (2008). Diagnosis and treatment of Wilson disease: An update. American Association for Study of liver diseases (AASLD). *Hepatology*, *47*(6), 2089–2111.

Scholefield, M., Church, S. J., Xu, J., Patassini, S., Roncaroli, F., Hooper, N. M., Unwin, R. D., & Cooper, G. J. S. (2021). Widespread decreases in cerebral copper are common to Parkinson's disease dementia and Alzheimer's disease dementia. *Frontiers in Aging Neuroscience*, *13*, 641222.

Scholefield, M., Unwin, R. D., & Cooper, G. J. S. (2020). Shared perturbations in the metallome and metabolome of Alzheimer's, Parkinson's, Huntington's, and dementia with Lewy bodies: A systematic review. *Ageing Research Reviews*, *63*, 101152.

Stankiewicz, J. M., Neema, M., & Ceccarelli, A. (2014). Iron and multiple sclerosis. *Neurobiology of Aging*, *35*(Suppl 2), S51–S58.

Stephenson, E., Nathoo, N., Mahjoub, Y., Dunn, J. F., & Yong, V. W. (2014). Iron in multiple sclerosis: Roles in neurodegeneration and repair. *Nature Reviews. Neurology*, *10*(8), 459–468.

Szklarczyk, D., Franceschini, A., Wyder, S., Forslund, K., Heller, D., Huerta-Cepas, J., Simonovic, M., Roth, A., Santos, A., Tsafou, K. P., Kuhn, M., Bork, P., Jensen, L. J., von Mering, C. (2014). STRING v10: Protein–protein interaction networks, integrated over the tree of life. *Nucleic Acids Research*, *43*(D1), D447–D452.

Tyanova, S., Temu, T., Sinitcyn, P., Carlson, A., Hein, M. Y., Geiger, T., Mann, M., & Cox, J. (2016). The Perseus computational platform for comprehensive analysis of (prote) omics data. *Nature Methods*, *13*(9), 731–740.

Uitti, R. J., Rajput, A. H., Rozdilsky, B., Bickis, M., Wollin, T., & Yuen, W. K. (1989). Regional metal concentrations in parkinson's disease, other chronic neurological diseases, and control brains. *The Canadian Journal of Neurological Sciences*, *16*, 310–314.

Vercellino, M., Masera, S., Lorenzatti, M., Condello, C., Merola, A., Mattioda, A., Tribolo, A., Capello, E., Mancardi, G. L., Mutani, R., Giordana, M. T., & Cavalla, P. (2009). Demyelination, inflammation, and neurodegeneration in multiple sclerosis deep gray matter. *Journal of Neuropathology and Experimental Neurology*, *68*(5), 489–502.

Walter, U., Wagner, S., Horowski, S., Benecke, R., & Zettl, U. K. (2009). Transcranial brain sonography findings predict disease progression in multiple sclerosis. *Neurology*, *73*(13), 1010–1017.

Ward, R. J., Zucca, F. A., Duyn, J. H., Crichton, R. R., & Zecca, L. (2014). The role of iron in brain ageing and neurodegenerative disorders. *Lancet Neurology*, *13*(10), 1045–1060.

Wickham, H., Averick, M., Bryan, J., Chang, W., McGowan, L. D., François, R., Grolemund, G., Hayes, A., Henry, L., Hester, J., Kuhn, M., Pedersen, T. L., Miller, E., Bache, S. M., Müller, K., Ooms, J., Robinson, D., Seidel, D. P., Spinu, V., Takahashi, K., ... Yutani, H. (2019). Welcome to the tidyverse. *The Journal of Open Source Software*, *4*(43), 1686.

Yu, S. P. (2003). Regulation and critical role of potassium homeostasis in apoptosis. *Progress in Neurobiology*, *70*(4), 363–386.

Zecca, L., Stroppolo, A., Gatti, A., Tampellini, D., Toscani, M., Gallorini, M., Giaveri, G., Arosio, P., Santambrogio, P., Fariello, R. G., Karatekin, E., Kleinman, M. H., Turro, N., Hornykiewicz, O., & Zucca, F. A. (2004). The role of iron and copper molecules in the neuronal vulnerability of locus coeruleus and substantia nigra during aging. *Proceedings of the National Academy of Sciences of the United States of America*, *101*(26), 9843–9848.

Zecca, L., Youdim, M. B., Riederer, P., Connor, J. R., & Crichton, R. R. (2004). Iron, brain ageing and neurodegenerative disorders. *Nature Reviews Neuroscience*, *5*(11), 863–873.

Zhang, L., Zheng, Y., Xie, J., & Shi, L. (2020). Potassium channels and their emerging role in parkinson's disease. *Brain Research Bulletin*, *160*, 1–7.

Zhang, Y., Bilbao, A., Bruderer, T., Luban, J., Strambio-De-Castillia, C., Lisacek, F., Hopfgartner, G., & Varesio, E. (2015). The use of variable Q1 isolation windows improves selectivity in LC-SWATH-MS acquisition. *Journal of Proteome Research*, *14*, 4359–4371.

Zucca, F. A., Capucciati, A., Bellei, C., Sarna, M., Sarna, T., Monzani, E., Casella, L., & Zecca, L. (2023). Neuromelanins in brain aging and Parkinson's disease: Synthesis, structure, neuroinflammatory, and neurodegenerative role. *IUBMB Life*, *75*, 55–65.

## SUPPORTING INFORMATION

Additional supporting information can be found online in the Supporting Information section at the end of this article.

---

**How to cite this article:** Carmona, A., Carboni, E., Gomes, L. C., Roudeau, S., Maass, F., Lenz, C., Ortega, R., & Lingor, P. (2024). Metal dyshomeostasis in the substantia nigra of patients with Parkinson's disease or multiple sclerosis. *Journal of Neurochemistry*, *168*, 128–141. https://doi.org/10.1111/jnc.16040